Atmos. Meas. Tech. Discuss., 6, 1771–1813, 2013
www.atmos-meas-tech-discuss.net/6/1771/2013/
doi:10.5194/amtd-6-1771-2013

Atmospheric Measurement Techniques
Discussions
Open Access

Detection of convective initiation using Meteosat SEVIRI: implementation in and verification with the tracking and nowcasting algorithm Cb-TRAM

D. Merk[1,*] **and T. Zinner**[1]

[1]Meteorologisches Institut, Ludwig-Maximilians-Universität, Theresienstr. 37, 80333 Munich, Germany
[*]now at: Leibniz-Institut für Troposphärenforschung, Permoserstr. 15, 04318 Leipzig, Germany

Received: 23 December 2012 – Accepted: 24 January 2013 – Published: 14 February 2013

Correspondence to: D. Merk (merk@tropos.de)

Published by Copernicus Publications on behalf of the European Geosciences Union.

Abstract

In this paper a new detection scheme for Convective Initation (CI) under day and night conditions is presented. The new algorithm combines the strengths of two existing methods for detecting Convective Initation with geostationary satellite data and uses the channels of the Spinning Enhanced Visible and Infrared Imager (SEVIRI) onboard Meteosat Second Generation (MSG). For the new algorithm five infrared criteria from the Satellite Convection Analysis and Tracking algorithm (SATCAST) and one High Resolution Visible channel (HRV) criteria from Cb-TRAM were adapted. This set of criteria aims for identifying the typical development of quickly developing convective cells in an early stage. The different criteria include timetrends of the 10.8 IR channel and IR channel differences as well as their timetrends. To provide the trend fields an optical flow based method is used, the Pyramidal Matching algorithm which is part of Cb-TRAM. The new detection scheme is implemented in Cb-TRAM and is verified for seven days which comprise different weather situations in Central Europe. Contrasted with the original early stage detection scheme of Cb-TRAM skill scores are provided. From the comparison against detections of later thunderstorm stages, which are also provided by Cb-TRAM, a decrease in false prior warnings (false alarm ratio) from 91 to 81 % is presented, an increase of the critical success index from 7.4 to 12.7 %, and a decrease of the BIAS from 320 to 146 % for normal scan mode. Similar trends are found for rapid scan mode. Most obvious is the decline of false alarms found for synoptic conditions with upper cold air masses triggering convection.

1 Introduction

Due to their hazardous impact, such as strong winds, hail or lightning thunderstorms remain a great threat to economy and society. Especially for the aviation industry the phenomenon carries a high financial risk; Mecikalski et al. (2002) and Murray (2002) stated that their annual costs related to thunderstorms exceed tens of millions of dollars.

Therefore interest is high to predict thunderstorms as early and precisely as possible. Although todays numerical weather prediction models are able to predict the likelihood for thunderstorms occurence in a specified area reliably, it is difficult to forecast the exact time and place and path of individual thunderstorms with numerical weather prediction (NWP) models alone.

NWP models have to deal with nonlinear dynamic processes acting on short time scales and limited spatial resolution that makes it necessary to parameterize convective processes. Improving spatial resolution (< 4 km) during the last years made it possible for NWP models to treat convection explicitly. Although a more physically meaningful lifecycle is reached, NWP models still do not necessarily show better point-forecasts. Furthermore constraints exist because of limited computer power. Therefore it is necessary to nest high-resolution domains into lower-resolution ones (Done et al., 2004; Tang et al., 2012). Even models resolving convective processes directly require exact measurements of small scale moisture distribution and flow kinematics. Crook (1996) showed that the initiation process of deep convection is highly dependent on the vertical moisture and temperature gradient. A shift of 1 K could already make the difference between Convective Initation and no occurance of convection.

As a result nowcasting, i.e. the extrapolation of existing developments based on observational data, is used to predict the development and path of individual thunderstorms. Nowcasting is made possible by means of remote sensing data with good spatial and temporal coverage. Useful data is provided by radar, satellites, or lightning networks. Outside Europe and North America radar data typically lacks coverage and is affected by ground echoes especially in mountainous areas. For the detection of convective cells in a very early stage – the Convective Initation (CI) – radar data is not very useful as precipitation echoes are not observable at that stage. Although additional methods exist for the detection of earlier development using radar, like the detection of convergence lines using Bragg scattering effects due to thermodynamical gradients or Rayleigh-scattering due to small insects (Weckwerth and Parsons, 2006; Wilson and Mueller, 1993), satellite data is better suited for this task. Mecikalski et al.

AMTD
6, 1771–1813, 2013

(2010) found that lead times of up to 75 min for thunderstorms are possible when a set of different channel criteria for geostationary satellite data is applied. Advantage of the geostationary perspective is the continous spatial and temporal coverage of wide regions. For the Meteosat Spinning Enhanced Visible and InfraRed Imager (SEVIRI) 12 different channels are available at image refresh rates of 15 min for normal scan mode and 5 min for rapid scan mode.

Different nowcasting tools were developed throughout the last years. While some concentrate on the tracking of mature thunderstorms such as RDT (Morel and Sénési, 2002) or MASCOTTE (Carvalho and Jones, 2001), others use radar data only, e.g. CONRAD (Lang, 2001) or RadTRAM (Kober and Taffener, 2009). There also exist nowcasting algorithms for the detection of CI, e.g. SATCAST (Mecikalski and Bedka, 2006). In addition to the detection of later development stages, a day-time detection of convection at an early or Convective Initiation stage is part of Cb-TRAM (Thunderstorm – Cb – Tracking an Monitoring, Zinner et al., 2008, 2013). Reinhardt and Dotzek (2010) investigated the quality of CI detections for both SATCAST and Cb-TRAM and found rather high false alarm ratios (see Sect. 3.1) which can be explained by the physical characteristics of convection. In the following study a combination of SATCAST and Cb-TRAM is conducted to merge the strengths of both methods to detect Convective Initiation within Cb-TRAM.

Through the work described in this manuscript Cb-TRAM is provided with a day and night-time detection of early convection stages and an estimate of the CI detection skill is obtained with a verification setup utilizing the detection of later stages within Cb-TRAM for normal and rapid scan Meteosat data. The tools on which the new detection scheme is based are described in Sect. 2. The development of the new detection and verification schemes as well as a detailed description are presented in Sect. 3. The verification including a comparison of the existing Cb-TRAM CI detection and the new algorithm as well as the comparison of 15 and 5 min Meteosat data is presented in Sect. 4. Afterwards a summary of the method and results and a discussion of the remaining sources of uncertainty is given in Sect. 5.

2 Tools for the detection of convective initation

The new detection scheme builds on two existing algorithms for the detection of convective clouds based on geostationary satellite data. The Cumulonimbus Tracking and Monitoring (Cb-TRAM) algorithm is introduced in Zinner et al. (2008) and changes to the detection schemes are presented in Zinner et al. (2013). The Satellite Convection Analysis and Tracking (SATCAST) is described by Mecikalski and Bedka (2006). In the following a short overview of these two algorithms is given.

2.1 Cb-TRAM

The Cumulonimbus Tracking and Monitoring (Cb-TRAM) is an algorithm for the detection, tracking and nowcasting of intense convective cells using the data from Meteosat SEVIRI. Cb-TRAM contains three core components: (1) the derivation of a motion vector field based on the Pyramidal Matching algorithm, (2) the detection of convective cells at different stages of their life cycle and (3) the tracking and nowcasting up to 60 min using the motion vector field. It is used in the EU projects RiskAware (2004–2006), FLYSAFE (2006–2009, Tafferner et al., 2008) and ongoing DLR project "Wetter und Fliegen" (Forster and Tafferner, 2009, 2012).

The calculation of the motion vector field depends on two consecutive satellite images. From these a disparity vector field $\boldsymbol{V}$ is derived by warping one image on the other so that either the differences of the image intensities are minimised or the local correlation is maximised. This optical flow method considers the typical autocorrelation of clouds in the sense that small scale cloud movement is dominated by the large scale flow pattern. Technically this is implemented through an analysis on different levels of spatial resolution. A first analysis on reduced horizontal resolution (large scale motion) is successively refined in succeeding steps down to the single pixel level. The use of this detailed motion field enhances, on the one hand, the tracking precision for small cells, and on the other hand, allows to calculate reliable local cooling or warming trends for cloud tops as apparent trends due to advection can be removed. Generally, local

AMTD
6, 1771–1813, 2013

time trends are calculated by subtracting the image at time t from a warped version of the image at $t-1$. As the disparity vector fields do not only include cloud motion, but also the changes in cloud amount, it is necessary to use slightly different timesteps or other channels to obtain an advection corrected result (see Zinner et al., 2008).

Cb-TRAM discriminates convective clouds at three different development stages. Stage 1 is called “early development“ or “Convective Initiation“ and covers only cloud elements showing strong vertical and/or horizontal growth. These clouds are characterized by fast cloud top cooling in infrared channels and increased reflectivity in the visible channels. To this end the local trend of cloud pixels in the IR10.8 and the High Resolution Visible (HRV) channels are investigated. That means, the convective cell has not necessarily reached a precipitation stage to be classified as “Convective Initiation“.

Stage 2 uses the cooling trend in the WV6.2 channel to detect convective cells displaying “rapid development” in the upper tropospheric region. “Mature thunderstorm” constitute the third stage. Mature convective cells typically show a cirrus anvil and a cloud top close to the top of the troposphere (or lower level inversions) or even “overshoots” over these levels. Stage 3 is mainly detected by a calculation of the a difference field between the WV6.2 and the IR10.8 channels. An additional criterion used therein that improves the limitation of the detection to active convective cores is the HRV channels texture using a normalised local standard deviation field (WV6.2 channel texture at nighttime).

The tracking of Cb-TRAM provides a log file containing the life cycle of individual cell objects. The tracking is based on overlap of detected cells in consecutive images. Existing cell objects at time $t-1$ are extrapolated using the disparity vector before the overlap with cells of time t is analysed. If no overlap is detected, the cell object of time t is considered a new cell object. If more than one cell object overlaps with exactly one cell object at the current timestep, a maximum overlap decision is made. Only the cell objects’ life cycle that shows the maximum area overlap is continued. Other cell objects’ life cyles end. If one cell object from $t-1$ overlaps with more than one object

AMTD
6, 1771–1813, 2013
Detection of convective initiation using Meteosat SEVIRI
D. Merk and T. Zinner

of time t, again maximum overlap provides the continuation of one cell life cycle and several new cell objects.

2.2 SATCAST

SATCAST was initially developed for the GOES 11 and 12 data, but also first efforts have been made to use Meteosat SEVIRI. The algorithm aims at providing early warnings of thunderstorms. To this end it combines three main components to detect Convective Initiation. The first is a convective cloud mask interpolated to 1 km resolution. The second component derives mesoscale atmospheric motion vectors and the third investigates actual brightness temperatures and multispectral timetrends. Convective initiation in SATCAST is defined as the first detection of radar reflectivities ≥ 35 dBZ equivalent to heavy precipitation produced by convective clouds. In their study Mecikalski and Bedka (2006) investigate the precursor signals for Convective Initiation and therefore the applied criteria can be directly compared to Cb-TRAM's early stage detection supposed to show signals prior to heavy precipitation.

The convective cloud mask splits the satellite scene into four different cloud types: (1) immature cumulus defined as warm clouds ($> -20\,^{\circ}$C) with pronounced texture (standard deviation of brightness counts), (2) thick stratus or thin cirrus that shows both little texture and warm cloud top temperatures, (3) thick cirrus, i.e. cold clouds ($< -20\,^{\circ}$C) with little texture and (4) cumulonimbus which typically shows cold cloud top temperatures and high texture in their active centre. This classification is achieved through a series of analyses considering the typical characteristics of convective clouds in the visible channels which are high brightness values and distinct cloud edges, the different appearance of Convective Initiation and Cb/thick cirrus in the IR10.8 channel and WV6.5-IR10.8 channel difference, the different appearance of stratus and Cb in terms of texture.

Atmospheric motion vectors (AMV) are calculated to derive cloud top cooling trends considering the cloud advection. As a basis serves the UW-CIMSS algorithm to derive motion vectors on synoptic scales important for assimilation of NWP models. To this

AMTD
6, 1771–1813, 2013

end, SATCAST investigates the satellite image for distinct cloud features that could be tracked over a defined time sequence and applies a a cross-correlation technique (Merrill et al., 1991) for matching these features. This method depends on high time repeat frequencies of satellite images. Changes to this algorithm were applied in order to provide motion vectors including both synoptic scale and mesoscale vectors. The latter being associated with Cumulus cloud ageostrophic motions. Quality checks applied within the UW-CIMSS algorihm result in a loss of mesoscale, ageostrophic motion vectors. The quality checks compares the satellite derived motion vectors with a NWP model first guess and checks the spatial connection of neighboured motion vectors. Therefore motion information on smaller scales is lost. To deal with this issue the following relexations to the original UW-CIMSS algorithm were applied in order to yield the more dense mesoscale atmospheric motion vector (MAMV) field: reduction of the NWP first guess constraint as subgrid motions can not be resolved reliable by the model; changes of feature selection and vector editing schemes so that horizontal resolution of feature box size and vertical resolution are increased. By this relaxation a 20 times greater number of vectors is achieved, but also including errorenous vectors that can result in unreliable cooling or warming trends.

Assuming that past trends continue into the future, the eight interest fields (see Table 1) are used to detect pixels with a high chance of further convective development. For the different channel values, channel differences, and derived time trends fixed tresholds are set.

For interest fields (1) and (4) the special importance of the freezing level is considered. It was found by Mueller et al. (2003) and Roberts and Rutledge (2003) that radar echoes of 5 and 35 dBZ were observed 15 and 30 min after the cloud top temperature dropped below the freezing point. Consequently there seems to be a direct connection between the fact that the freezing level is reached and the development of rain. A possible explanation is the Bergeron–Findeisen process which takes place for super-cooled clouds where ice and super-cooled droplets coexist and is known to be of high importance for the formation of precipitation.

AMTD
6, 1771–1813, 2013

Interest Field (2) refers to the vertical cloud growth which results in cloud top cooling. This can be measured by a satellite if one assumes that a cloud is an ideal black body, which is a valid assumption for optically thick clouds. At the beginning of the development process warm cloud top temperatures are observed that show fast cooling within a short time due to vertical growth. Reasonable cooling rates for CI detection are found by Roberts and Rutledge (2003) and are between −4 and −8 K within 15 min for weak and strong growth rates, respectively.

Interest Field (3) tests for persistence of cloud growth to assure that the observed cooling is not only a random pattern. Therefore one additional timestep is considered. It is required that the cooling rate over two timesteps is greater than the cooling rate for one timestep. This criterion allows for weakening or increasing cooling rates over time as only the persistence of vertical cloud growth is tested here.

For interest field (5) the channel difference of the water vapour channel WV6.5 and the infrared window channel IR10.7 is calculated. This gives information about the cloud top-height relative to the troposphere or a very dry mid- to upper-layer in the troposphere. For a clear sky atmosphere the warm surface temperatures are observed via the IR10.7 channel. In the WV6.5 channel the main signal originates from the water vapour in the middle to upper troposphere between 500 hPa and 200 hPa. Radiation from lower layers is absorbed and re-emitted at the temperature of higher layers. Therefore the temperature difference of WV6.5-IR10.7 is negative for clear sky conditions. For a developing cumulus cloud (CI) the difference becomes less negative as higher clouds typically show cooler cloud top temperatures at IR10.7. At later stages of the convective life cycle the difference becomes even slightly positive when the cloud reaches and overshoots the tropopause (corresponding to the "mature thunderstorm" detection of Cb-TRAM).

Thus for a developing convective cloud the negative difference decreases with time. This is utilised in interest field (7) where the time trend of the channel difference is calculated. This time trend becomes positive as higher negative difference values at

AMTD
6, 1771–1813, 2013

time $t-1$ are subtracted from lower negative difference values at time t. Higher positive values refer to stronger development in terms of vertical growth.

Interest Fields (6) and (8) use the so-called split-window channel, usually used to detect cirrus clouds, volcanic ash and deep convection. Here it is used to highlight cloud pixels that are likely to develop into a precipitating cloud. It was found that near-zero differences are observed for convective rainfall regions.

In Mecikalski and Bedka (2006) 7 out of 8 met criteria per pixel are required to issue a CI warning. 60 to 70 % accuracy was found for three cases over the US for different synoptic forcing regimes. For other areas than the mid-latitudes, especially in areas where the process of warm-rain takes place, i.e. the tropics further adjustments may be needed.

Mecikalski et al. (2010) also investigated the use of the additional channels provided by Meteosat SEVIRI and found 21 out of 67 initially defined IR channel differences and time trends to have the least amount of redundance for the investigation of cloud depth, updraft strength and cloud-top glaciation. As only preliminary tresholds for 123 cases are used in this study and further testing with a larger data set would be required for these interest fields, the Mecikalski et al. (2010) study is not used here. Only the eight original criteria listed above are considered in the following.

3 Development of an improved detection scheme for convective initation

The aim of the development of this new detection scheme for Convective Initiation is the combination of the strengths of existing detection algorithms in a way that the advance warning of strong convective cells is improved. To achieve this aim an analysis of strengths and weaknesses is necessary at first. Time trends are used for many detection criteria within SATCAST and Cb-TRAM. As the derivation of such trends is highly dependent on the accuracy of the calculated motion fields, the quality of these vector fields is of great importance.

The MAMVs in SATCAST require the existence of features that can be tracked reliably troughout a sequence of satellite images. The extension of the original MAMV algorithm which keeps track of mesoscale motion may result in erroneous vectors which could, accordingly, lead to unreasonable cooling trends. Especially for strong vertical wind shear conditions the accuracy of AMVs seems to drop, as outlined by Mecikalski et al. (2008).

The motion vector field in Cb-TRAM is derived on a pixel basis and is independent of trackable features. The disparity vector field in Cb-TRAM, of course, still comprises some weaknesses. The field does not only include the pure advection, but also local development which has to be considered correctly. Nonetheless, the matching algorithm in Cb-TRAM provides pixel-by-pixel motion fields for all clouds moving in a satellite scene derived in a physically meaningful, scale dependent way.

On the other hand, the Cb-TRAM CI detection is limited to one combination of criteria including the HRV. For this reason only daytime detection is possible. While the skill of the “mature thunderstorm” detection has been evaluated using lightning data (Zinner et al., 2013), a systematic evaluation of this first stage detection is pending. Opposed to this, SATCAST uses a set of interest fields with several channel’s information. Compared to Cb-TRAM this approach reduces the high sensitivity and uncertainty of a decision that depends on a single field. In addition the importance of individual interest fields for CI detection in SATCAST was already investigated by Mecikalski et al. (2008) which provides a starting point for the further implementation of selected interest fields into a new method.

Following from these considerations, we decided to include parts of the SATCAST based systematic set of criteria and thresholds into Cb-TRAM as new stage 1 “Convective Initiation/early development” detection scheme. This way, we aim to improve the efficiency of SATCAST criteria through the use of the Cb-TRAM disparity vector fields for an improved derivation of time trends. Additional objective of the following work is the provision of a day- and nighttime CI detection scheme for Cb-TRAM.

AMTD
6, 1771–1813, 2013

3.1 Verification method

In order to evaluate the skill of the detection for development stage 1 "early development/Convective Initiation" in Cb-TRAM a suitable verification method has to be defined.

Typically independent observational data should be used for validation purposes. For the verification of the correct detection of Convective Initiation lightning data, radar networks (precipitation data) or satellites (cloud data) could be considered. Although Convective Initiation can be accompanied by lightning and precipitation in the transition phase to mature Cumulonimbus, following our definition CI is usually preceding these phenomena. Due to the time shift and the related spatial shift between early signs and actual proof of convective activity, there is no data which provides a direct validation of a Convective Initiation detection. Thus it has to be evaluated considering such a shift, e.g. using a tolerance region in space and time (cf. Reinhardt and Dotzek, 2010).

Cb-TRAM provides an estimate of the development of CI events into more developed thunderstorms itself. It generates a connection between the stages "early development/Convective Initiation" and "rapid development" or "mature thunderstorms" via its tracking capability. We decided to use this feature for verification in the following. Although collected by the same sensor, this is at least partially independent data, as the detection schemes of stage 2 and stage 3 are providing information on later stages of development using different channel combinations. Cb-TRAM skill to detect mature thunderstorm clouds is evaluated in Zinner et al. (2013): the probability to detect an mature intense convective cell is about 77 %, at least during the day. At the same time only about 16 % of all stage 3 detections do not show any convective activity in terms of lightning. Similar to the verification in Zinner et al. (2013) an object based verification method is applied here, using the cell objects generated by Cb-TRAM and the related life-cycle log data for each cell. If the Cb-TRAM's CI detections are perceived as forecasts of further development into thunderstorms and stages 2 and 3 for the related

AMTD
6, 1771–1813, 2013

Cb-TRAM object as proof of convective development, one can define the following categorical variables regarding the development of each individual cell object:

- A hit H is a cell object at stage 1 that shows further development into stage 2 or 3 within 60 min.
- A false alarm F is a cell object at stage 1 that does not show further development within 60 min.
- A miss M is a cell object at stage 2 or 3 without any stage 1 detection during the previous 60 min.

This demand related to this definition is rather ambitious as the evaluation is done on an individual cell basis instead of an evaluation of the general affinity of a wide tolerance region to display further thunderstorm development. This has to be taken into account when comparing our values to less strictly defined verifications (e.g. Reinhardt and Dotzek, 2010; Mecikalski et al., 2008). Nonetheless, this definition complies to common sense and thus provides appreciable result values. It is well suited to compare the two CI algorithms within Cb-TRAM, and the results can be directly provided by the Cb-TRAM algorithm.

Using these categorical variables different verification statistics can be calculated. In this paper the following ones are used:

$$\mathrm{POD} = \frac{H}{H+M} \tag{1}$$

$$\mathrm{FAR} = \frac{F}{H+F} \tag{2}$$

$$\mathrm{CSI} = \frac{H}{H+M+F} \tag{3}$$

$$\mathrm{BIAS} = \frac{H+F}{H+M}. \tag{4}$$

Discussion Paper | Discussion Paper | Discussion Paper | Discussion Paper |

AMTD

6, 1771–1813, 2013

Detection of convective initiation using Meteosat SEVIRI

D. Merk and T. Zinner

The ideal value is 1 for the Probability of Detection (POD), Critical Success Index (CSI), and BIAS and is 0 for the False Alarm Ratio (FAR). POD and FAR should be considered as a pair. It is possible to improve the POD by just randomly increasing the number of forecast objects, but this would normally result in an synchronous increase of the FAR. The POD provides the fraction of correctly detected early developments when a thunderstorm followed the detection, while the FAR provides the fraction of detections which are not followed by thundestorms. The CSI combines both, the number of hits and the number of false alarms. Typically the CSI shows small values for rare events, like Convective Initiation or thunderstorms in general, as the number of hits is low. The BIAS simply gives the ratio of forecasted to observed number of events. Values of the BIAS above 1 constitute over-forecasting and below 1 under-forecasting. Nonetheless the BIAS does not judge how well observations and forecasts correspond.

A Cb-TRAM cell object can represent several consecutive cell life-cycles of a multi-cell thunderstorm, because the tracking algorithm will allocate a new development which lies close enough to the expected track to an already existing cell in a decaying stage. As a result more than one CI classification per cell object is possible. Consider the following example object history: 0 min – stage 3 detection (mature), 15 min – stage 3, 30 min – stage 3, 45 min – stage 1 (CI), 60 min – stage 2 (rapid development), 75 min – stage 3. This means that the cell life-cycle starts with a missed CI development, but nonetheless shows a hit at 45 min.

3.2 Convective cloud interest field mask

The first step of the new detection scheme is the limitation to an interest field for convective clouds within a full satellite scene. Similar to SATCAST's convective cloud mask only pixels within this interest field are evaluated further. This step aims at the reduction of false alarms that can be found in areas where the likelihood for convective clouds in the satellite image scence is minimal. The interest field is derived using three different tests:

AMTD
6, 1771–1813, 2013

- 253 K < IR10.8 < 278 K
- HRV Reflectivity > 0.5 (can be used only under daytime conditions)
- local standard deviation at WV7.3 and IR10.8 larger than defined treshold

The first test investigates the cloud top temperature in the IR10.8 channel. Clouds with top temperatures < 253 K typically have reached higher altitudes so that it is likely for those clouds to be either Cb or thick Cirrus. It is very unlikely for Convective Initiation to show top temperatures below this threshold value. The same treshold is used within SATCAST to seperate mature from initial convective clouds. Cloud top temperatures above 278 K refer to very low clouds such as cumulus or stratus. SATCAST uses 273 K as one typical criterion for Convective Initiation. This value is relaxed here to account for a wider range of convective developments.

Test two is adapted from Cb-TRAM. Only those pixels with a reflectivity higher than the given treshold are considered for Convective Initiation. Convective clouds typically are bright due to their high optical thickness. Lower values of reflectivity are most likely caused by thinner clouds or scattered cloudiness in a given pixel (e.g. mostly very small cumulus).

A distinct signal of cumulus clouds that is taken into account for the third test is their lumpy appearance. The convective process does not produce a smooth cloud top structure which is more likely for, e.g. cirrus and stratus. Although the HRV channel would provide the best horizontal resolution to detect such variability, the IR10.8 and WV7.3 are used here to provide a method applicable day and night. While the IR10.8 channel gives the possibility to detect all clouds in the lower troposphere (if no overlaying clouds in the upper layer exists) the WV7.3 is used to guarantee that clouds have reached a significant altitude at a lower mid-troposphere level (approx. 3000 m). The localized standard deviation (cf. Zinner et al., 2008) is calculated for a local area around each pixel using a Gaussian kernel. Threshold values are derived by mean values of the detected CI objects within the existing Cb-TRAM version. Separate masks of these

AMTD
6, 1771–1813, 2013

three tests are presented in Fig. 1 for a case over the Iberian Peninsula together with the resulting interest field for both day- and nighttime conditions.

3.3 Scoring system

As for SATCAST a scoring system is adopted for a set of criteria for CI detection with a final decision based on the number of met criteria. A basic set of six criteria is selected from SATCAST by means of a statistical analysis and some general considerations. For MSG SEVIRI channel IR10.8 is used instead of IR10.7 onboard GOES, and WV6.2 instead of WV6.5. Criteria with proven value for CI detection are prefered (i.e. the eight SATCAST GOES criteria). For these criteria tested treshold values exist and can be used immediately. An additional criterion is the processing time requirement as a nowcasting tool, of course, should provide results quickly. Thus the number of utilized channels and followingly detection criteria is limited to a minimum while preserving the best possible result. Beforehand some of the SATCAST interest field tresholds have been modified. For IF 2 the IR10.8 cooling rate is set to −6 K within 15 min (compare Tables 1 and 2). Reasonable cooling rates for CI detection following Roberts and Rutledge (2003) are between −4 and −8 K within 15 min for weak and strong growth rates, respectively. The timeframe in IF 3 for which the temperature dropped below the freezing point is set to 15 min referring to the founding by Roberts and Rutledge (2003) that 15 min after this criteria is fulfilled first convective radar echoes can be observed.

In analogy to the study by Mecikalski et al. (2008), an analysis for different criteria combinations was performed for an independent training dataset, including three days in summer (9 June 2009, 3 July 2009, 19 July 2009) from 07:00 to 17:00 UTC. The eight SATCAST criteria (Table 1) and the existing Cb-TRAM criterion are used in combination with the convective cloud interest field mask. The criteria are split into four groups with different physical basis to limit the combination of needed tests as listed in Table 2. Group 1 describes the infrared cooling trend, Group 2 the relative height to the tropopause and Group 3 the split window channel test with the individual time trends, respectively. Group 4 is the Cb-TRAM detection for Convective Initiation investigating

HRV brightening and IR10.8 cooling. The statistical analysis is described in detail in Sect. 3.1. Similar to the study of Mecikalski et al. (2008) 15 possible combinations of the four groups were investigated. The best trade-off concerning CSI and FAR was yield for the combination of group 1, group 2 and group 4. The criteria in group 3 aim to detect clouds that are already glaciated and therefore are in a very final phase of Convective Initiation. Due to the slightly different emphasis on early development and, consequently, the fact that such development is already covered by the stage 2 detection within Cb-TRAM and the result of the combinations, we decided to omit these criteria for our purposes. Finally the set of six different criteria from groups 1, 2 and 4 as listed in Table 3 is used to further investigate the pixels in the previously derived interest field mask.

At daytime conditions five of six criteria have to be met at a given time for a given pixel to consider this pixel to show Convective Initiation. At nightime the five remaining IR criteria have to be met (without the criterion 6). Further a minimum object size is required. Only CI pixels which have at least two neighbouring pixels are kept. This is analoguous to the other Cb-TRAM detection schemes and is mainly used to avoid false alarms related to very small short-lived objects.

4 Skill of CI detection: verification within Cb-TRAM

In the following section the verification method described in Sect. 3.1 is applied on normal scan and rapid scan Meteosat SEVIRI data for a representative number of days. For a clearer appreciation of the results the skills are always presented in comparison to the original stage 1 detection scheme in Cb-TRAM.

AMTD
6, 1771–1813, 2013

4.1 Test cases and conditions

The verification is carried out for seven different test days over the area of mid europe. These days can be classified into three different, typical synoptic weather conditions for thunderstorm development:

- cold front passage: 26 May 2009 (day 1), 6 June 2010 (day 2), 3 July 2010 (day 3) and 14 July 2010 (day 4)
- advection of upper cold air: 14 July 2010 (day 4) and 12 June 2009 (day 5)
- high pressure conditions: 25 June 2010 (day 6) and 29 June 2010 (day 7)

For all test scenarios the same configuration in Cb-TRAM is used. The analysed area lies between −9.5 and 11.5° longitude and 36.5 and 55.5° latitude. As the area investigated covers whole mid europe, for some of these days a clear distinction of synoptic regimes is not easy. The classification is done by adressing the most dominant synoptic feature of the individual test days. For example, the 14 July 2010 shows influence of a cold front and backward upper cold air masses triggering convection. The latter feature is the more dominant (more convective cells for this feature) here. Thus, in the further investigation this day is classified as a "cold air" case. In Fig. 3 an example comparison between the current and the new CI detection is given for this test case on 14 July 2010. For evaluation of daytime conditions the timeframe between 07:00 and 17:00 UTC is used. For nighttime conditions two individual timeframes between 00:00 to 07:00 and 17:00 to 23:45 (23:55 for rapid scan mode) are used for each day. For 29 June 2010 the rapid scan datasets are incomplete over a longer timeperiod and this day is therefore not included in the statistics.

AMTD
6, 1771–1813, 2013

Detection of convective initiation using Meteosat SEVIRI

D. Merk and T. Zinner

4.2 Verification results

4.2.1 Normalscan

The results for daytime conditions in normal scan mode are investigated as total values over all seven test days, as sub-totals for the three synoptic conditions and for each test day individually. This is done to get an overall impression of the new detection algorithm compared to the existing one and to explore the behaviour under different synoptic weather conditions. The total values as listed in Table 4 show an increase in hits by 4 using the new algorithm instead of the existing one, a decrease in false alarms by 3108 and a increase in misses by 84. This manifests an improvement, but has to be put into perspective. POD (Eq. 1), FAR (Eq. 2), CSI (Eq. 3) and BIAS (Eq. 4) also shown in Fig. 4 do all reflect this improvement.

The striking charcteristic of both CI detections, as well as CI detection skill in general, is obviously a large false alarm ratio around 90 % (and related, a large BIAS) while the probability of detection is 45 % at best. At this point it must be emphasized that this is, on the one hand, owed to the choice of rather conservative verification definitions (Sect. 3.1), on the other hand, it is inherent to the involved physics. Usually a single thunderstorms strong updraft is preceeded by a number of early less confined convective developments, but our verification allows only an allocation of one CI development to one thunderstorm. From a whole area that shows signs of early development, usually only one development is selected by very localized characteristics and the preferred updraft will soon dominate all other early developments as low level convergence and upper level divergence suppresses other updrafts. Consequently a large number of false alarms has to be expected. The mediocre POD is in part simply owed to the multi-cell nature of most storms in the analysis. Early development of a secondary cell is often masked by the preceeding older cell's later life-cycle stages.

The percentage of thunderstorms that are preceeded by a previous detection of Convective Initiation, i.e. receive an advance warning, shows only a small change from 29 to 28 % over all days (POD). The most striking improvement is a nearly halfed

AMTD
6, 1771–1813, 2013

absolute number of false alarms (5427 → 2319). The FAR decreases from 91 to 81 %. For the reasons mentioned above, this is still a high absolute number, and is reflected in the clear over-forecasting tendency (BIAS still larger 146 %). Nonetheless, in the framework of different development detections in Cb-TRAM this makes sense. Although, the specific CI detection might not carry a high probability to develop further, still an accumulation of CI detection in certain regions should be regarded as a warning sign.

The CSI, combining False Alarms, Hits and Misses, increases from 7 to 13 %, a significant near-doubling of CSI. This improvement in the overall forecasting behaviour also is reflected in the decrease of the overforecasting tendency from 320 to 146 %. Therefore, although still noisy, a clearer signal of potentially dangerous convective developments is provided by the new algorithm.

In the day-by-day analysis in Fig. 4 it can be seen that best day's FAR is around 76 % and POD around 45 %, worst day's FAR at 95 % and POD at 15 %. BIAS does show a peak value at 12 June 2009 for both the new and previous detection scheme, while it does not vary much for the rest of the days. The newer method shows a higher or equal number of hits at 4 out of 7 days compared to the original CI detection, and a lower number of false alarms for all seven days. This results in a better FAR and CSI for all days and increased POD at 3 days. In order to take a closer look at the individual synoptic conditions, we have calculated total values for each synoptic class. In the following the individual day results are summarized first, afterwards a closer look at characteristics influences on the individual days is taken.

– A visual inspection (not shown) gives following typical cloud structures: for the class of "cold front" days there is a high amount of clouds visible, both convective (especially Cb) and non-convective (Cirrus or Stratus). Therefore the satellite-perspective on Convective Initiation along the front is limited (e.g. due to prevailing Cirrus shields of mature Cb). Typical for the class of "cold air" days is a honeycombed structure of many convective cells. Geostationary satellites provide a good view on Convective Initiation that is very widespread under these unstable atmospheric conditions. For the class of "high pressure" days fewer clouds are visible compared to the other two classes. Convection mainly depends on the time of day.

- For the grouped statistical values for each of the synoptic classes, the highest POD is found for high pressure cases, both for the previous and new detection algorithm. The greatest increase for the new algorithm is found for high pressure cases, followed closely by cold air cases. FAR in the previous algorithm is lowest for cold front cases. A possible explanation for this, at the first moment surprising result, is the more persistent dynamic convection trigger mechanism. This way the average very statistical nature of CI is reduced. For the new algorithm the FAR is lowest at high pressure cases followed closely by cold front cases. The greatest decrease in FAR is achieved for high pressure days. The best CSI values are found for high pressure followed by cold front cases with the new algorithm. The lowest BIAS value is found for cold front cases. The highest reduction of BIAS compared to the original algorithm is found for cold air cases (by nearly one third) where the influence of the 12 June 2009 is most striking.

- A closer look at this day shows convective cells over large parts of mid europe as a result from the advection of upper cold air masses, with the typical honeycomb structure of convective cells, but nearly no further development to stage 2 or 3 during the whole day. The original Cb-TRAM CI detection generates many false alarms and only three hits. The latter are connected with some scattered cells in Spain. The new detection algorihm detects one more hit, but it shows a drastic 16-fold decrease in false alarms. In this case it is obvious that the small number of hits distorts the significance of POD and FAR on this day. Although the number of false alarms decreases by 1133, i.e. decisively, the FAR only decreases by 5 %.

- The other day in this test sample which is worth consider more closely is the 3 July 2010 as this day provides a rather untypical increase in hits, compared to the other cold front and even all days evaluated. A visual inspection shows Convective Initiation primarily at a convergence line ahead of the front and a lot of

AMTD
6, 1771–1813, 2013

D. Merk and T. Zinner

CI objects over the Alps. An unobstructed satellite view on these developments together with the sustained lifting mechanism leads to many successful CI detections. The main difference to the original detection scheme seems to be the improved detection of orographically induced Convective Initiation, which results in an increased number of hits but also a reduction of false alarms.

- Although the synoptic classes are arranged by their dominant similarities, some special features can occur on individual days. The reduction of false alarms is especially high on the cold air day of 12 June 2009 and the two high pressure days, with the false alarms reduced to the third on 25 June 2010. A visual inspection shows that the eastern part of the domain on the latter day is also influenced by upper cold air masses.

Summarizing the cases with cold upper air masses, the criteria of the new CI detection algorithm result in a drastically reduced number of false alarms. But false alarms also decreased on the other test days on a significant level.

For nighttime conditions no direct comparison is possible due to the fact that the original CI algorithm did not provide detections at night. Therefore only the new results are investigated, again both for all test nights and for each night individually. In addition the nighttime detection skill can be evaluated by an application to the daytime data, i.e. only the the five IR criteria are used. As can be seen in Fig. 4, there is only a slight difference between day- and nighttime detection for FAR, CSI and BIAS compared to the improvements achieved by the new method. The main difference lies in a reduction in POD (excluding day 5), as expected due to the missing HRV information, but at the same time the FAR is slightly reduced also.

At nighttime over land a general decrease of convective activity is observed (as in this investigation). Missing radiation and a stable boundary layer result in unfavourable conditions for the formation of convection. Due to the lower activity at nighttime the values of POD, FAR and CSI show poorer values compared to daytime as early developments (CI) tend to “die out” over night. New forming convective cells are interrupted in their development cycle at nightfall if no dynamic trigger is active. This results in increased number of false alarms.

The total results over all test nights (00:00–07:00 UTC and 17:00–00:00 UTC) a POD of 13 %, a FAR of 90 % and a CSI of 6 % was found. The POD, CSI and FAR values for most days are very similar, except day 5. This day shows a very high FAR and a low POD. This can be explained by the very small number of cases in these values. Nearly no convective activity occurs during this night due to missing forcing. Consequently the number of false alarms is the smallest of all nights, too. In the high pressure cases a visual inspection provides the trend of decreasing CI activity after sunset. Altough this is the case, referring to the best POD and FAR values for high-pressure situations, these seem to give the best possibility to detect remaining cells. Considering the longer timeframe for night (14 h) and that activity on the night onset may be still higher than later at night, the tendency of decreasing activity at nighttime can be seen by the smaller number of hits and misses (representing the total active cells). In our set of test days also some days with nighttime forcing are present. An example for a cell development at nighttime observed with the new detection algorithm in Cb-TRAM is given in Fig. 5. New convective cells over the Black Forest and the Jura Mountains develop after sunset. In general, the CI detection at nighttime is most promising when synoptic dynamic or orographic triggers are present.

4.2.2 Rapidscan

In SEVIRI rapid scan mode the repeat cycle for new satellite images is 5 min instead of 15 min. Therefore a three times better temporal coverage is reached compared to normal scan. It seems obvious that this should improve the possibility to detect and track especially rapidly changing cloud processes such as Convective Initiation. This should therefore manifest in a higher number of detected hits. In the following a comparison of the results of the rapid scan CI detections using the original and the new detection scheme is presented first. The basis are six of the seven test days presented for the normal scan analysis before. Data for 29 June 2010 shows to many gaps and is

AMTD
6, 1771–1813, 2013

omitted therefore. The eventual benefits of rapid scan versus normal scan are explored afterwards.

For rapid scan mode some slight modifications in the detection algorithms were made (see Table 3) to account for the better time resolution. These include (1) investigating trend values in IF 1 and IF 5 over the last 5 min instead of last 15 min using adapted treshold values for this shorter timeframe, (2) sustained cooling in IF 2 is considered for the last 15 instead of 30 min, (3) Cb-TRAM rapidscan threshold for IF 6 is used. For normal scan mode at least 30 min (2 timesteps) have to be considered for sustained cooling criteria, while for rapid scan we can use shorter intervals. With the founding by Roberts and Rutledge (2003) that after 15 min the first precipitation is observed under sustained cooling conditions, we think that in this way setting IF 2 to 15 min we get a physical meaningful combination of the two criteria for detecting strong convective cells in an early stage. Verification is done using the same 60 min timeframe for further developments of cells, but now given the chance to verify this using 5 min timesteps.

Due to the increase of investigated timesteps the total number of investigated cell objects also increases as many more short lived developments can be observed in the 15 min time period between the two normal scan observations. Under daytime conditions the results for the sum of all six rapid scan test days show an increase of hits by 465, a decrease of false alarms by 22 908 (relative decrease of more than 60 %) and an increase in misses comparing the original with the new CI algorithm. The latter is a technical side effect which results from an increased number of stage 2 and 3 cell objects. Although the detection for stage 2 and 3 is not modified here, the changes of the stage 1 detection do also influence the former as these also include all neighboring pixels of lower stages. So in some cases more individual stage 2 or 3 cells occur resulting in a higher amount of misses. This also distorts POD, CSI and BIAS trough the increase of misses. It was especially observed under rapid scan conditions that one bigger missed stage 3 cell object in the previous algorithm is counted as, e.g. three

AMTD

6, 1771–1813, 2013

individual smaller stage 3 objects in the new algorithm. But it is also an issue in normal scan mode.

This also leads to the slight decrease of POD on 4 of 6 days although number of hits increases on 5 days. FAR decreases from 96 to 86 %, CSI clearly increases from 4 to 11.5 % and is therefore nearly 3 times better than before. BIAS decreases from 999 to 295 % and so overforecasting is three times less. The number of hits increases for 4 out of the 6 days while 2 show a decrease. False alarm numbers are improved for all 6 days, so that in some cases only about 10 % of the original false alarms remain (12 June 2009).

Taking a look at the synoptic classes, it is found that best values of POD (around 50 % for rapid scan) were found for both algorithms for the high pressure day as in the normal scan case. Although absolute hit numbers are increasing the discussed technical issue with misses cells results in an decrease of POD for two classes when applying the new detection method. With a near doubling of hits, the biggest increase in POD is yield for cold air cases here. Best FAR values for the previous algorithm were found for cold front cases, applying the new algorithm for the cold air cases. The improvement in FAR for the latter one is also the best under all three classes. The same is true for the CSI values. This supports the normal scan results where also the FAR improved mainly for the upper cold air mass conditions.

If one compares day and night results in Fig. 4, it is obvious that the overall behaviour of FAR, POD, CSI and BIAS does not show any major differences between day and night – although the trend of decreasing convection during night hours found for normal scan is supported by the results for rapid scan.

More interesting than the comparison of original and new CI detection for rapid scan data is, of course, the question whether the use of rapid scan data automatically improves the skill of the detection compared to the normal scan data for the test days in both analyses.

One advantage of the rapid scan over the normal scan mode is the possibilty to evaluate the development each 5 min. As we assigned some of the criteria from Mecikalski

AMTD
6, 1771–1813, 2013

and Bedka (2006) to 5 min with an adjusted threshold we have the chance to observe rapidly developing cells. The higher-resolution also gives us the chance to evaluate the development over more individual timesteps within a longer-timeperiod (last 15 min). This has a direct positive influence e.g. on IF 2 as sustained cooling can be validated in 5 min steps. The higher time resolution gives the possibilty to better detect and verify rapid developments and short-living cells that may be obscured using only 15-min timesteps. This is expressed within the results in the higher amount of hits, misses and false alarms compared to the normal scan and also in terms of BIAS. Even with the overall increase of detectable cells in rapid scan mode we achieved a lower BIAS compared to the BIAS value in normal scan mode using the previous algorithm. Therefore a forecaster using the new algorithm will get a clearer picture of the situation updated each 5 min. Comparing BIAS for the new algorithms in normal and rapid scan mode overforecasting is still a factor of 2 higher in rapid scan mode. Explanations being very fast developing cell objects not covered in stage 1 by the normal scan (higher number of hits) and higher chance of detecting false alarms simply by more timesteps observed. The latter often being detections visible for only one timestep and most likely result from wrong motion vectors. Referring to statistical skill values when comparing the new algorithm in normal and rapid scan mode the results are higher POD values for the three synoptic classes in rapid scan mode but FAR and CSI only better for the cold air class. With the drastically decreasing number of false alarms and the omission of tracking all these cells we also obtain an improvement in calculation time. This is an important goal for a nowcasting tool aimed for real-time-warnings.

5 Conclusions

By combination of the strengths of two existing detection algorithms (Cb-TRAM by Zinner et al., 2008 and SATCAST by Mecikalski and Bedka, 2006) for geostationary satellite data, a new detection scheme for Convective Initiation has been developed and implemented in Cb-TRAM. A set of criteria from the SATCAST CI detection, using thermal infra-red channel measurements for one point in time as well as derived time trend, has been combined with detailed cloud motion and deformation fields from the Cb-TRAM pyramidal matching algorithm. In the latter an optical flow based method is of special importance for the derivation of detailed cloud top cooling trends. A pixel-by-pixel analysis of six different CI tests using the channels WV6.2, IR 10.8, and during daytime including the HRV became possible this way. In order to reduce the number of false detections decisively, an additional pre-selection of convective clouds with an interest field mask excludes all areas with non-convective clouds.

The convective cloud interest field mask is limited to clouds which are cold, bright, and show enough small scale texture (in IR10.8, in HRV, and in WV7.3 and IR10.8, respectively). On this interest field mask, the set of six CI criteria aims to assess the typical signatures of quickly developing convective cells at an early stage, such as strong updrafts resulting in strong cloud top cooling and increasing cloud top height.

Two criterions use IR10.8 time trends over different periods of time. The drop of temperatur below freezing level is analysed, as well as the value of the difference between WV6.2 and IR10.8 and their time trend. Finally the original Cb-TRAM criterion for Convective Initiation is included which requires simultaneous brightening in the HRV and cooling in the IR10.8. A scoring system connects different criteria: pixels are considered to display Convective Initiation in a satellite scene if five out of six possible criteria are met during daytime; at nighttime all five infra-red criteria have to be met.

For the analysis of the skill of the original and the newly developed methods, a verification of the Convective Initiation detections against later stages of the convective life-cycle has been used. For that purpose the further development to the subsequent life-cycle stages “rapid cooling” and “mature thunderstorm” within Cb-TRAM has been investigated. Cb-TRAM cell objects which show further development after Convective Initiation detection within 60 min are considered a hit, missing further development a false alarm, and a missing Convective Initiation detection within 60 min before further development a miss. By means of probability of detection (POD), false alarm ratio

(FAR), critical success index (CSI), and BIAS seven test days and -nights are analysed both for normal- and six for rapid scan METEOSAT SEVIRI data.

The main results are as follows:

– FAR for normal scan mode under daytime conditions decreases from 91 to 81 % and CSI increases from 7.4 to 12.7 % while BIAS is reduced from 320 to 146 % using the new detection algorithm instead of the original Cb-TRAM method. Thus an improvement for all these statistical verification values is reached. POD decreases slightly altough the number of detected hits are increasing due to a technical side effect concerning detection of misses in Cb-TRAM.

– Considering each day individually FAR and CSI shows improvement for each day, POD for three out of seven days.

– The CI detection newly implemented in Cb-TRAM shows a reduction of false alarms for all test days both for normal scan (15 min data) and rapid scan (5 min) when compared to the original detection.

– The decline in false alarms is most prominent for synoptic conditions with upper cold air masses that produce a lot of convective cells in normal and rapid scan mode.

– An important improvement within Cb-TRAM is the fact that the new algorithm works during day and night: POD, FAR and CSI at night are of the same order of magnitude as during the day. A comparison of day (including HRV criterion) and night-time detection (only IR criteria) during the daytime hours reveals mainly an increase of POD through the use of the HRV information.

Generally the high values of FAR for most of the days lead to the question on the limitations of the detection of Convective Initiation using geostationary data only and their use as an early warning for stronger convective storm development. The statistical character of convection has to be considered. Only a small part of a large number of CI candidate cumuli will develop into mature thunderstorms as the most intense cell will suppress surrounding development through its impact on surface convergence and upper level divergence. In addition, not each cumulus cloud satisfying the typical criteria for fast growth for some time, develops into a cumulonimbus during its life-cycle. Unfavourably conditions for further development as the interruption of a sufficient supply of warm moist air, a stable layer at some height above the convective cloud top, or the advection of the whole cell into an area with unfavourable conditions for convection could stop the development at any time of the cell life-cycle.

Together with the choice of the verification method this all sets narrow boundaries for the quality values possible. Since the verification is done by investigating the further development against the detections for "rapid developement" and "mature thunderstorm" within Cb-TRAM, the results also depend on the quality of these detections. For 77 % of all "mature thunderstorm" objects an overlap with lightning was found in Zinner et al. (2013). Although some cell objects within an area of rapidly growing cumulus clouds may be classified as false alarms in a conservative individual cell based verification setup, as presented here, it could be as legitimate to classify a whole area of multiple CI detections as hits, if only one single strong thunderstorm develops out of the area. Walker et al. (2012) implemented a object based tracking based on Zinner et al. (2008) and verified the cell objects against radar data. Taking into account all of the cell objects he received a POD value of 32 % comparable to our outcome. The FAR of 55 % is lower than in our study but has to be put into perspective. Walker et al. (2012) uses a manual search in the surrounding area which is less strict than our automated tracking.

While the number of hits did increase only slightly for some of the days, the decline of false alarms is the clearest improvement as far as the comparison to the original CI detection within Cb-TRAM is concerned. As shown, this decrease is more pronounced for days with upper cold air masses. These days do strongly influence the total values for all days. The omission of tracking false alarm cells also results in an improvement of calculation time. The calculated statistical values of POD, FAR and CSI and BIAS

AMTD
6, 1771–1813, 2013

depend on the numbers of hits, misses and false alarms. Especially for a low total number of observed objects these skill values tend to be very sensitive to small changes of the latter categorial variables.

Calculations for different synoptic groups depend on the possibility to distinguish synoptic patterns for the whole domain. Although this was possible for most of the days used here, mixed situations occur (e.g. 14 July 2010). Longer time series would be desireable to corroborate the results found in this study.

The detection of Convective Initiation in general is highly dependent on cloud top cooling trends. These, on the other hand, rely on the disparity vector field. Advection of optical thin cirrus clouds over cumulus clouds can lead to apparent cloud top cooling values which are not an effect of rising cloud tops. Although the presented method uses an optical flow method, incorrect vectors within the field can obviously not be ruled out. This may lead to situations where false alarms are diagnosed which are actually only an effect of erroneous cooling trends and not thunderstorms.

Due to the geostationary position of Meteosat satellites, the best horizontal resolution is available at the equator, decreasing with higher latitudes. For Europe this results in a reduced horizontal resolution by a factor of about 1.5. The actual resolution for HRV is about 1.5 km × 1.5 km and 4 km × 6 km for the standard resolution Meteosat channels for europe. Therefore few details are visible which are of particular importance for small scale developments like Convective Initiation.

The oblique viewing angle around 50° also affects the observation of cloud tops. More and more cloud side information influences the measured signal and the derived cloud top temperatures. Therefore the tresholds suggested by Mecikalski and Bedka (2006) may be slightly shifted for higher latitudes. Using strict tresholds does also not account for developments just below these given limits and thus some hits can be missed.

Considering the difficulties arising when detecting and verifying Convective Initiation this leads to the question on how these could be further improved. Investigating microphysical properties for convective clouds at/near the cloud top using satellite data as

AMTD
6, 1771–1813, 2013

done by Mecikalski et al. (2011) could improve the understanding of in-cloud processes during convection and therefore help to find typical patterns that can be used for CI detection. Application of stability data fields provided by satellites or numerical weather model outputs may help in reducing the amount of false alarms. One can also think of other strategies to combine different criteria for CI detection, e.g. using fuzzy logic as in Cb-TRAM. Another approach for verification could be to soften the cell perspective and verify whole areas where Convective Initiation takes place.

Acknowledgements. EUMETSAT and DLR Oberpfaffenhofen are acknowledged for providing SEVIRI data. We thank Dennis Stich for the fruitful discussions. This manuscript is dedicated to the memory of our colleague Hermann Mannstein who died unexpectedly and much too early on 25 January 2013. He was a scientific innovator behind many cloud remote sensing activities at DLR over nearly three decades. Among many other things, he developed the Cb-TRAM core algorithms. He will be deeply missed as expert, adviser and friend.

References

Carvalho, L. and Jones, C.: A satellite method to identify structural properties of mesoscale convective systems based on the maximum spatial correlation tracking technique (MASCOTTE), J. Appl. Meteorol., 40, 1683–1701, 2001. 1774

Crook, N. A.: Sensitivity of moist convection forced by boundary layer processes to low-level thermodynamic fields, Mon. Weather Rev., 124, 1768–1785, 1996. 1773

Done, J., Davis, C. A., and Weisman, M.: The next generation of NWP: explicit forecasts of convection using the weather research and forecasting (WRF) model, Atmos. Sci. Lett., 5, 110–117, doi:10.1002/asl.72, 2004. 1773

Forster, C. and Tafferner, A.: An integrated user-oriented weather forecast system for air traffic using real-time observations and model data, in: Proceedings of the European Air and Space Conference (CEAS), 26–29 October 2009, Manchester, UK, 2009. 1775

Forster, C. and Tafferner, A.: Nowcasting Thunderstorms for Munich Airport, DLR-Forschungsbericht, Deutsches Zentrum für Luft- und Raumfahrt e.V., Bibliotheks- und Informationswesen, Köln, 2012. 1775

AMTD

6, 1771–1813, 2013

Detection of convective initiation using Meteosat SEVIRI

D. Merk and T. Zinner

Title Page
Abstract | Introduction
Conclusions | References
Tables | Figures
◀| |▶
◀ ▶
Back | Close
Full Screen / Esc
Printer-friendly Version
Interactive Discussion

Kober, K. and Taffener, A.: Tracking and nowcasting of convective cells using remote sensing data from radar and satellite, Meteorol. Z., 1, 75–84, 2009. 1774
Lang, P. (Ed.): Cell tracking and warning indicator derived from operational radar products, in: Proceedings of the 30th International Conference on Radar Meteorology, Munich, Germany, 2001. 1774
Mecikalski, J. R. and Bedka, K. M.: Forecasting convective initiation by monitoring the evolution of moving cumulus in daytime GOES imagery, Mon. Weather Rev., 134, 49–78, 2006. 1774, 1775, 1777, 1780, 1795, 1796, 1800
Mecikalski, J. R., and Coauthors: Aviation applications for satellite-based observations of cloud properties, convection initiation, in-flight icing, turbulence, and volcanic ash, B. Am. Meteorol. Soc., 88, 1589–1607, doi:10.1175/BAMS-88-10-1589, 2007 1772
Mecikalski, J. R., Bedka, K. M., Paech, S. J., and Litten, L. A.: A statistical evaluation of GOES cloud-top properties for nowcasting Convective Initiation, Mon. Weather Rev., 136, 4899–4914, 2008. 1781, 1783, 1786, 1787
Mecikalski, J. R., MacKenzie Jr., W. M., Koenig, M., and Muller, S.: Cloud-top properties of growing cumulus prior to Convective Initiation as measured by Meteosat second generation, Part I: Infrared fields, J. Appl. Meteorol. Clim., 49, 521–534, 2010. 1773, 1780
Mecikalski, J. R., Watts, P. D., and Koenig, M.: Use of Meteosat second generation optimal cloud analysis fields for understanding physical attributes of growing cumulus clouds, Atmos. Res., 102, 175–190, 2011. 1801
Merrill, R. T., Menzel, W. P., Baker, W., Lynch, J., and Legg, E.: A report on the recent demonstration of NOAA's upgraded capability to derive satellite cloud motion winds, B. Am. Meteorol. Soc., 72, 372–376, 1991. 1778
Morel, C. and Sénési, S.: A climatology of mesoscale convective systems over Europe using satellite infrared imagery, I: Methodology, Q. J. Roy. Meteorol. Soc., 128, 1953–1971, 2002. 1774
Mueller, C. K., Saxen, T., Roberts, R., Wilson, J., Betancourt, T., Dettling, S., Oien, N., and Yee, J.: NCAR Auto-Nowcast system, Weather Forecast., 18, 545–561, 2003. 1778
Murray, J. J.: Aviation weather applications of Earth Science Enterprise data, Earth Observ. Mag., 11, 27–30, 2002. 1772
Reinhardt, B. and Dotzek, N.: Validation of the MSG Convection Initiation Product (Final Report), Tech. Rep., EUMETSAT Contract EUM/CO/09/4600000642/MK, available from: EUMETSAT, 2010. 1774, 1782, 1783

AMTD
6, 1771–1813, 2013

Detection of convective initiation using Meteosat SEVIRI

D. Merk and T. Zinner

Roberts, R. D. and Rutledge, S.: Nowcasting storm initiation and growth using GOES-8 and WSR-88D data, Weather Forecast., 18, 562–584, 2003. 1778, 1779, 1786, 1794

Tafferner, A., Forster, C., Senesi, S., Guillou, Y., Laroche, P., Delannoy, A., Lunnon, B., Turb, D., Hauf, T., and Markovic, D.: Nowcasting thunderstorm hazards for flight operations: the Cb-WIMS approach in FLYSAFE, in: Proc. 26th Int. Congress of the Aeronautical Sci. (ICAS), 14–19 September 2008, Anchorage, Alaska, 2008. 1775

Tang, Y., Lean, H. W., and Bornemann, J.: The benefits of the Met Office variable resolution NWP model for forecasting convection, Meteorol. Appl., doi:10.1002/met.1300, in press, 2012. 1773

Walker, J. R., MacKenzie, W. M., Mecikalski, J. R., and Jewett, C. P.: An enhanced geostationary satellite-based Convective Initiation algorithm for 0–2-h nowcasting with object tracking, J. Appl. Meteorol. Climatol., 51, 1931–1949, doi:10.1175/JAMC-D-11-0246.1, 2012. 1799

Weckwerth, T. M. and Parsons, D. B.: A review of Convection Initiation and motivation for IHOP2002, Mon. Weather Rev., 134, 5–22, 2006. 1773

Wilson, J. W. and Mueller, C. K.: Nowcasts of thunderstorm initiation and evolution, Weather Forecast., 8, 113–131, 1993. 1773

Zinner, T., Mannstein, H., and Tafferner, A.: Cb-TRAM: tracking and monitoring severe convection from onset over rapid development to mature phase using multi-channel Meteosat-8 SEVIRI data, Meteorol. Atmos. Phys., 101, 191–210, 2008. 1774, 1775, 1776, 1785, 1796, 1799

Zinner, T., Forster, C., de Coning, E., and Betz, H.-D.: Validation of the METEOSAT storm detection and nowcasting system Cb-TRAM with lightning network data – Europe and South Africa, Atmos. Meas. Tech. Discuss., 6, 1269–1310, doi:10.5194/amtd-6-1269-2013, 2013. 1774, 1775, 1781, 1782, 1799

AMTD

6, 1771–1813, 2013

Table 1. SATCAST GOES-11 interest fields (IF) for the detection of Convective Initiation.

IF	criteria	treshold
1	10.7 µm T_B	$< 273\,K$
2	10.7 µm T_B trend	$< -4\,K\ (15\,min)^{-1}$
3	10.7 µm T_B trend	$\Delta T_B\ (30\,min)^{-1} < \Delta T_B\ (15\,min)^{-1}$
4	10.7 µm T_B drop below 273 K	within prior 30 min
5	(6.5–10.7) µm	−10 K to −35 K
6	(12.0–10.7) µm	−3 K to 0 K
7	(6.5–10.7) µm trend	> 3 K
8	(12.0–10.7) µm trend	> 2 K

AMTD
6, 1771–1813, 2013

D. Merk and T. Zinner

Table 2. Grouped set of criteria for CI detection.

criteria	critical value
Group 1 (IR10.8 cooling trend)	
10.8 µm T_B trend	$< -6\,\mathrm{K}\,(15\,\mathrm{min})^{-1}$
10.8 µm T_B trend	$\Delta T_B\,(30\,\mathrm{min})^{-1} < \Delta T_B\,(15\,\mathrm{min})^{-1}$
T_B in 10.8 µm drop below 273 K	within last 30 min
Group 2 (relative height within troposphere and growth)	
(6.2–10.8) µm	−10 K to −35 K
(6.2–10.8) µm trend	> 3 K
Group 3 (split window channel test)	
(12.0–10.8) µm	−3 K to 0 K
(12.0–10.8) µm trend	> 2 K
Group 4 (Cb-TRAM CI detection)	
HRV × 10.8 µm	Cb-TRAM treshold

AMTD
6, 1771–1813, 2013

D. Merk and T. Zinner

Table 3. Set of six criteria used for the new CI detection algorithm together with the individual tresholds for normal and rapid scan mode.

#	criteria	critical value (NS)	critical value (RS)
1	10.8 µm T_B time trend	$< -6\,\mathrm{K}\,(15\,\mathrm{min})^{-1}$	$< -2\,\mathrm{K}\,(5\,\mathrm{min})^{-1}$
2	10.8 µm T_B time trend	$\Delta T_B\,(30\,\mathrm{min})^{-1} < \Delta T_B\,(15\,\mathrm{min})^{-1}$	$\Delta T_B\,(15\,\mathrm{min})^{-1} < \Delta T_B\,(10\,\mathrm{min})^{-1} < \Delta T_B\,(5\,\mathrm{min})^{-1}$
3	10.8 µm T_B drop below 273 K	within last 15 min	
4	(6.2–10.8) µm	−10 K to −30 K	−10 K to −30 K
5	(6.2–10.8) µm time trend	> 3 K	> 1 K
6	HRV × 10.8 µm	Cb-TRAM NS threshold	Cb-TRAM RS threshold

AMTD
6, 1771–1813, 2013

Detection of convective initiation using Meteosat SEVIRI

D. Merk and T. Zinner

Table 4. Categorical variables and statistics under daytime (07:00–17:00 UTC) conditions for the old and the new algorithm (old → new). Listed are the results for normalscan and rapidscan mode for each of the test days as well as the results for the three synoptic classes. Hits, misses and false alarms are given as absolute numbers, POD, FAR, CSI and BIAS are expressed as a percentage. For each of the synoptic classes the average (av.) values are given.

nr	date	Hits	False Alarms	Misses	POD (in %)	FAR (in %)	CSI (in %)	BIAS (in %)
				Normalscan mode				
all days (total)		538 → 542	5427 → 2319	1329 → 1413	28.8 → 27.7	91.0 → 81.0	7.4 → 12.7	320 → 146
cold front (av.)		85 → 90	598 → 359	250 → 262	25.4 → 25.6	87.6 → 80.0	9.1 → 12.7	204 → 128
1	26 May 2009	80 → 69	616 → 329	347 → 375	18.7 → 15.5	88.5 → 82.7	7.7 → 8.9	163 → 89
2	6 Jun 2010	53 → 48	471 → 253	127 → 141	29.4 → 25.4	89.9 → 84.0	8.1 → 10.9	291 → 159
3	3 Jul 2010	121 → 153	707 → 494	275 → 269	30.6 → 36.3	85.4 → 76.4	11.0 → 16.7	209 → 153
cold air (av.)		34 → 36	960 → 238	115 → 115	22.9 → 23.8	96.6 → 86.9	3.1 → 9.3	667 → 182
4	14 Jul 2010	65 → 68	713 → 402	224 → 223	22.5 → 23.4	91.6 → 85.5	6.5 → 9.8	269 → 162
5	12 Jun 2009	3 → 4	1206 → 73	5 → 6	37.5 → 40.0	99.8 → 94.8	0.2 → 4.8	15113 → 770
high pressure (av.)		78 → 100	857 → 384	176 → 200	30.7 → 33.3	91.7 → 79.3	7.0 → 14.6	368 → 161
6	25 Jun 2010	81 → 64	933 → 323	98 → 119	45.3 → 35.0	92.0 → 83.5	7.3 → 12.7	567 → 212
7	29 Jun 2010	135 → 136	781 → 445	253 → 280	34.8 → 32.7	85.3 → 76.6	11.5 → 15.8	236 → 140
				Rapidscan mode				
all days (total)		1599 → 2064	35754 → 12846	2141 → 2987	42.8 → 40.9	95.7 → 86.2	4.1 → 11.5	999 → 295
cold front (av.)		348 → 396	5244 → 2506	466 → 614	42.8 → 39.2	93.8 → 86.4	5.7 → 11.3	687 → 287
1	26 May 2009	280 → 273	6191 → 2004	418 → 554	40.1 → 33.0	95.7 → 88.0	4.1 → 9.6	927 → 275
2	6 Jun 2010	191 → 215	3742 → 1791	342 → 430	35.8 → 33.3	95.1 → 89.3	4.5 → 8.8	737.9 → 311
3	3 Jul 2010	573 → 701	5799 → 3722	639 → 857	47.3 → 45.0	91.0 → 84.2	8.2 → 13.3	526 → 284
cold air (av.)		173 → 327	6395 → 1893	438 → 457	38.7 → 41.7	97.4 → 85.3	2.5 → 12.2	1469 → 283
4	14 Jul 2010	244 → 565	5093 → 2912	388 → 760	38.6 → 42.6	95.4 → 83.8	4.3 → 13.3	845 → 262
5	12 Jun 2009	101 → 88	7696 → 874	159 → 154	38.8 → 36.4	98.7 → 90.9	1.3 → 7.9	2999 → 398
high pressure (av.)		210 → 222	7233 → 1543	195 → 232	51.9 → 48.9	97.2 → 87.4	2.8 → 11.1	1838 → 389
6	25 Jun 2010	210 → 222	7233 → 1543	195 → 232	51.9 → 48.9	97.2 → 87.4	2.8 → 11.1	1838 → 389

AMTD
6, 1771–1813, 2013

Detection of convective initiation using Meteosat SEVIRI

D. Merk and T. Zinner

Table 5. Categorical variables and statistics under nighttime (00:00–07:00 UTC, 17:00–00:00 UTC) conditions for the new algorithm. Hits, misses and false alarms are given as absolute numbers, POD, FAR, CSI and BIAS are expressed as a percentage. For each of the synoptic classes the average (av.) values are given.

nr	date	Hits	False Alarms	Misses	POD (in %)	FAR (in %)	CSI (in %)	BIAS (in %)
	Normalscan mode							
–	all days	164	1543	1076	13.2	90.4	5.9	138
–	cold front (av.)	31	295	198	13.5	90.5	5.9	142
1	26 May 2009	20	195	190	9.5	90.7	5.0	102
2	6 Jun 2010	39	369	202	16.2	90.4	6.4	169
3	3 Jul 2010	34	322	202	14.4	90.5	6.1	151
–	cold air (av.)	11	171	89	11.0	94.0	4.1	182
4	14 Jul 2010	21	295	150	12.3	93.4	4.5	185
5	12 Jun 2009	1	47	27	3.6	98.0	1.3	171
–	high-pressure (av.)	25	158	153	14.0	86.3	7.4	103
6	25 Jun 2010	27	161	164	14.1	85.6	7.7	98
7	29 Jun 2010	22	154	141	13.5	87.5	6.9	108
	Rapidscan mode							
–	all days (total)	1275	10 968	2795	31.3	89.6	8.5	301
–	cold front (av.)	266	2375	589	31.1	89.9	8.2	309
1	26 May 2009	96	1786	542	15.0	94.9	4.0	295
2	6 Jun 2010	383	2755	692	35.6	87.8	10.0	292
3	3 Jul 2012	319	2585	533	37.4	89.0	9.3	341
–	cold air (av.)	173	1405	372	31.7	89.0	8.9	290
4	14 Jul 2010	256	1948	482	34.7	88.4	9.5	299
5	12 Jun 2009	89	862	259	25.6	90.6	7.4	273
–	high pressure (av.)	141	1032	285	33.1	88.0	9.7	275
6	25 Jun 2010	141	1032	285	33.1	88.0	9.7	275

AMTD
6, 1771–1813, 2013

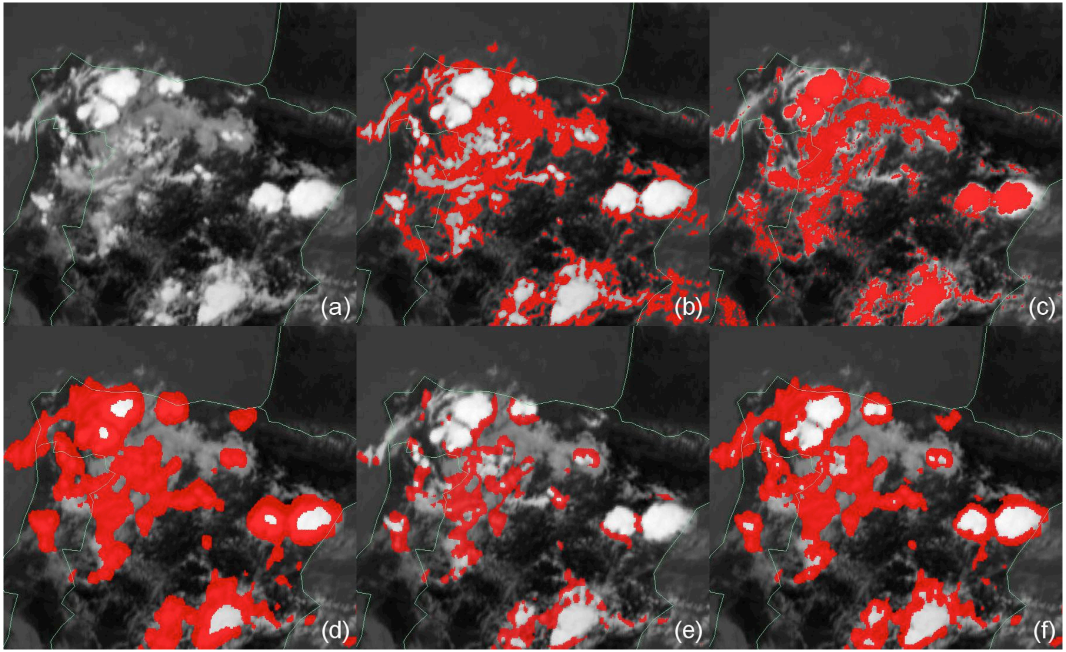

Fig. 1. Limitation to interest field: **(a)** IR10.8 cloud scene over Iberian Peninsula with various (convective) cloud types. Different tests for the convective cloud interest field masks: **(b)** $253\,\mathrm{K} < \mathrm{IR}10.8 < 278\,\mathrm{K}$, **(c)** $\mathrm{HRV} > 0.5$ **(d)** local standard deviation at WV7.3 and IR10.8 **(e)** interest field mask at daytime, **(f)** and nighttime condition (without HRV). Positive test results for each pixel are plotted in red.

AMTD
6, 1771–1813, 2013

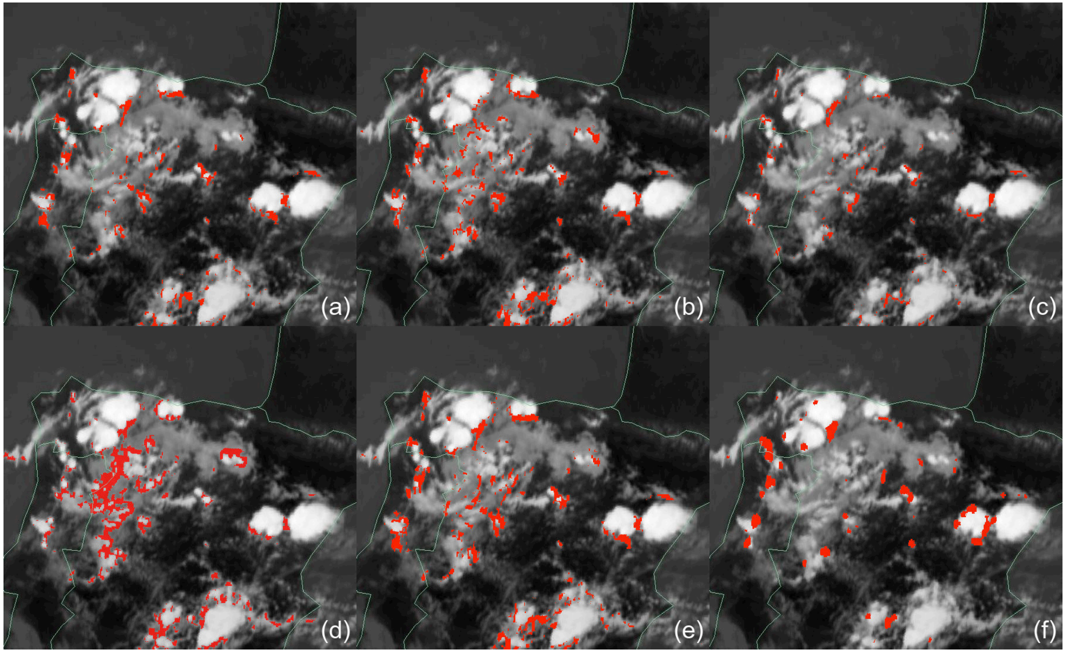

Fig. 2. Different masks for the six separate criteria listed in Table 3 for the same scene as in Fig. 1. Pixels plotted in red meet the individual tresholds for the defined criterion. **(a)** Criterion #1: 15 min IR10.8, **(b)** #2 30 min IR10.8, **(c)** #3 freezing level IR10.8, **(d)** #4: WV6.2-IR10.8, **(e)** #5: 15 min WV6.2-IR10.8, **(f)** #6: HRV × IR10.8.

AMTD
6, 1771–1813, 2013

Detection of convective initiation using Meteosat SEVIRI

D. Merk and T. Zinner

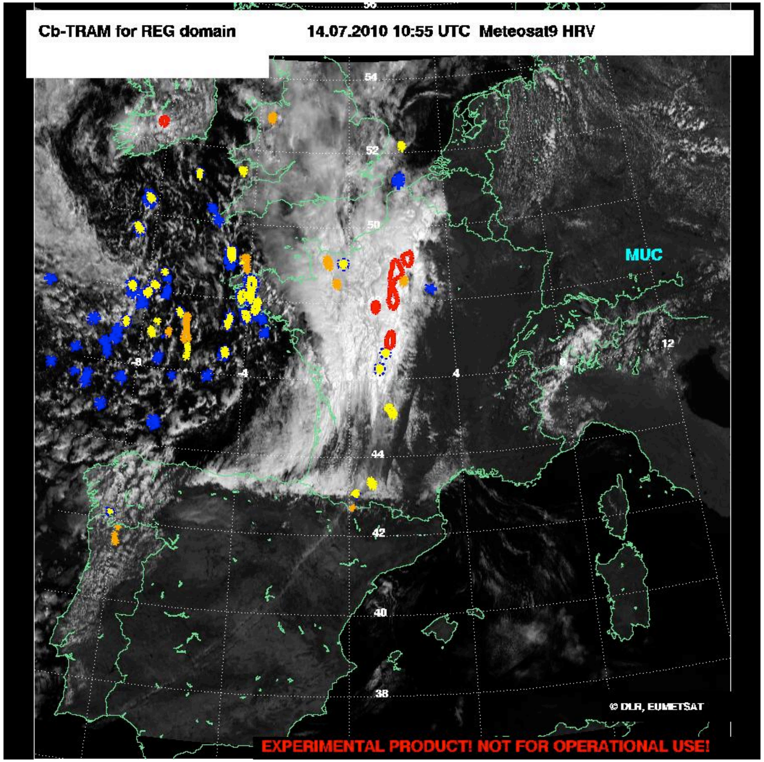

Fig. 3. Example of the test domain and Cb-TRAM for 14 July 2014. Yellow structures are CI objects detected by the new algorithm, blue structures are objects detected by the previous algorithm. Red and orange are the rapid development and mature Cb objects, respectively.

AMTD
6, 1771–1813, 2013

Detection of convective initiation using Meteosat SEVIRI

D. Merk and T. Zinner

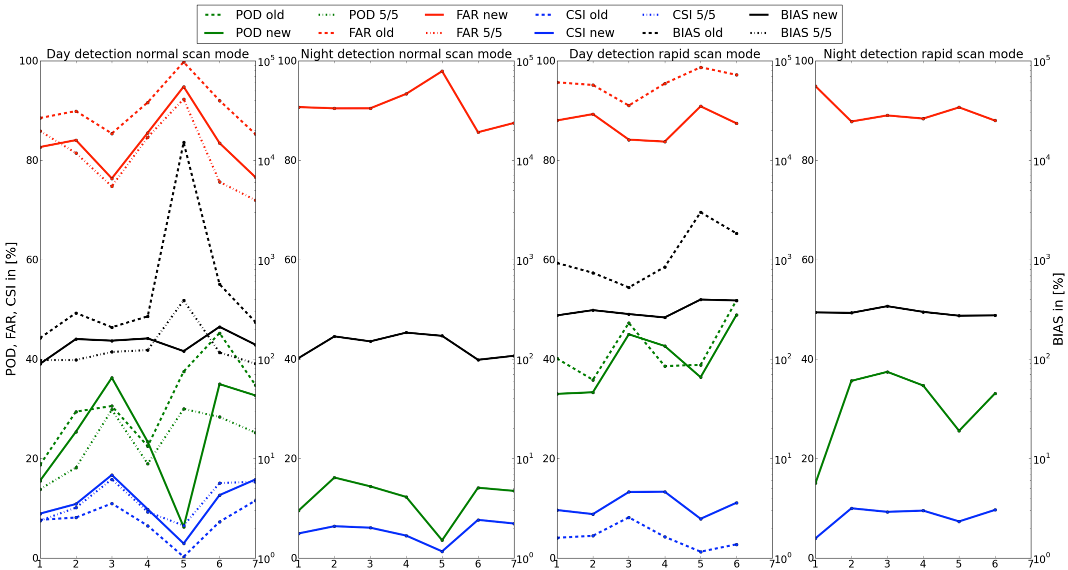

Fig. 4. POD, FAR, CSI and BIAS for the test days: green, red, blue and black lines, respectively. Dashed line mark the original CI detection algorithm results while the bold lines mark the new CI detection results, dotted lines in the left figure mark the new nighttime detection mode applied to the daytime data (using the five IR criteria only).

AMTD
6, 1771–1813, 2013

Detection of convective initiation using Meteosat SEVIRI

D. Merk and T. Zinner

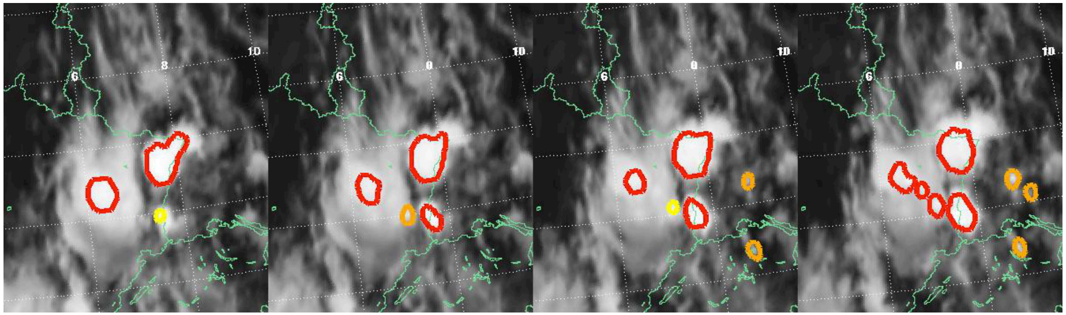

Fig. 5. Development of new thunderstorm cells in an orographic environment over the Black Forest and Jura Mountains in the night of 3 July 2010 between 22:30 UTC and 23:15 UTC. The plots show the cell objects als polygons in the same colors as in Cb-TRAM (yellow: convective Initiation, orange: rapid development, red: mature thunderstorm) on top of the IR10.8 satellite images.

AMTD
6, 1771–1813, 2013

Detection of convective initiation using Meteosat SEVIRI

D. Merk and T. Zinner